Simultaneous achievement of high perpendicular exchange bias and low coercivity by controlling ferromagnetic/antiferromagnetic interfacial magnetic anisotropy

Cite as: J. Appl. Phys. **121**, 073902 (2017); https://doi.org/10.1063/1.4976568
Submitted: 07 November 2016 • Accepted: 01 February 2017 • Published Online: 17 February 2017

Yu Shiratsuchi, Wataru Kuroda, Thi Van Anh Nguyen, et al.

Simultaneous achievement of high perpendicular exchange bias and low coercivity by controlling ferromagnetic/antiferromagnetic interfacial magnetic anisotropy

Yu Shiratsuchi,[1,a)] Wataru Kuroda,[1] Thi Van Anh Nguyen,[1] Yoshinori Kotani,[2] Kentaro Toyoki,[1,2] Tetsuya Nakamura,[2] Motohiro Suzuki,[2] Kohji Nakamura,[3] and Ryoichi Nakatani[1]

[1]*Department of Materials Science and Engineering, Graduate School of Engineering, Osaka University, 2-1 Yamadaoka, Suita, Osaka 5650871, Japan*

[2]*Japan Synchrotron Radiation Research Institute (JASRI)/SPring-8, 1-1-1 Kouto, Sayo, Hyogo 6795198, Japan*

[3]*Department of Physics Engineering, Mie University, 1577 Kurimamachiya, Tsu, Mie 514-8507, Japan*

(Received 7 November 2016; accepted 1 February 2017; published online 17 February 2017)

This study investigates the influence of Pt and Au spacer layers on the perpendicular exchange bias field and coercivity of Pt/Co/(Pt or Au)/Cr_2O_3/Pt films. When using a Pt-spacer, the perpendicular exchange bias was highly degraded to less than 0.1 erg/cm^2, which was about half that of the Au-spacer system. The Au spacer also suppressed the enhancement in coercivity that usually occurs at around room temperature when using Pt. It is suggested that this difference in exchange bias field is due to in-plane interfacial magnetic anisotropy at the Pt/Cr_2O_3 interface, which cants the interfacial Cr spin from the surface normal and results in degradation in the perpendicular exchange bias. *Published by AIP Publishing*. [http://dx.doi.org/10.1063/1.4976568]

INTRODUCTION

In a spin valve film,[1] a representative spintronic device, antiferromagnetic (AFM) and ferromagnetic (FM) materials play an important role in inducing exchange bias via magnetic anisotropy at the FM/AFM interface. The unidirectional nature of this exchange bias causes it to manifest itself as a shift in the magnetization curve along the magnetic-field axis.[2–4] When the exchange bias field exceeds the coercivity, the FM magnetization direction is fixed at a certain direction when the magnetic field is zero. Under ideal conditions, the exchange bias field should be as high as possible and the coercivity near zero; however, when exchange bias is induced in actual systems, the coercivity is often enhanced.[3–5] It is therefore important to achieve a high exchange bias while simultaneously maintaining a low coercivity.

Modern spintronic devices are designed so that any magnetization or spin is aligned perpendicular to the film plane to ensure integration, high speed operation, and low power consumption. The perpendicular exchange bias that is necessary to meet the requirements for future spintronics has been reported in several systems, such as $[Co/Pt]_5/(Co + CoO)$,[6] $[Co/MnPd]_{10}$ multilayers,[7] $[Pt/Co]_4/Pt/Fe\text{-}Co/MnIr$,[8] and Pt/Co/$Cr_2O_3$.[9,10] In some of these systems, a spacer layer such as Pt is inserted at the FM/AFM interface to control/enhance the exchange bias field,[11–13] and this sometimes gives rise to the enhancement in coercivity mentioned above. In a previous report relating to a Pt/Co/Cr_2O_3/Pt stacked system, a high perpendicular exchange anisotropy energy density, J_K exceeding 0.4 erg/cm^2, was achieved.[14] It was also found that by inserting a Pt spacer layer at the Co/Cr_2O_3 interface, the blocking temperature of the exchange bias could be increased,[13] which resulted in a decrease in exchange bias field and increase in coercivity. Another promising feature of perpendicular exchange bias using Cr_2O_3 is its magnetoelectric ability, wherein the polarity of the exchange bias is made switchable by the application of an electric field.[10,15–20] This device concept is based on the FM magnetization switches that accompany a reversal in exchange bias polarity,[21] and so both a high exchange bias field and low coercivity are obviously essential. In this study, we show that a high perpendicular exchange bias and low coercivity can be simultaneously achieved by utilizing a Au spacer layer and discuss the results in relation to the spin orientation at the FM/AFM interface.

EXPERIMENTAL

The films studied were fabricated using a DC magnetron sputtering system with a base pressure below 5×10^{-6} Pa. The typical stacking structure of the films was Pt(1.2, 2.0)/Co(0.4, 0.6)/X(= Pt, Au)(0.5)/Cr_2O_3(150)/Pt(20)/α-Al_2O_3(0001)-substrate unless otherwise specified. The numbers in parenthesis represent the thickness of each layer in nanometers. The Pt buffer layer was deposited at room temperature and annealed for 1 hour at 873 K to smooth its surface. Onto this, a Cr_2O_3 layer was deposited at 773 K by reactive sputtering. The Au or Pt spacer layer, Co layer, and Pt capping layer were deposited in sequence onto the Cr_2O_3 layer at room temperature. As the sputtering gas, a pure Ar for Pt, Au, and Co, and an Ar + O_2 gas mixture for Cr_2O_3 were used. The gas pressure during deposition was 0.5 Pa for Pt and Cr_2O_3, 0.6 Pa for Co, and 0.8 Pa for Au.

Structural characterizations were carried out using reflection high-energy electron diffraction (RHEED), X-ray diffraction (XRD), and X-ray reflectivity (XRR). The RHEED

[a)]Author to whom correspondence should be addressed. Electronic mail: shiratsuchi@mat.eng.oska-u.ac.jp

observations were carried out *in-situ* in a chamber directly connected to the deposition chamber. The magnetic properties were characterized by means of a vibrating sample magnetometer (VSM), magneto-optic Kerr effect (MOKE) magnetometer, and soft and hard X-ray magnetic circular dichroism (XMCD). Magnetization curves were recorded at room temperature by using VSM with magnetic-fields applied perpendicular and parallel to the film plane. The MOKE loops were measured with a polar configuration, which is sensitive to the perpendicular component of magnetization. All MOKE measurements were carried out at a temperature between 80 and 300 K after cooling the sample from above the Néel temperature (310 K) under a magnetic field of −4 kOe. Soft- and hard-X-ray absorption spectroscopy (XAS) and XMCD spectroscopy, both of which are element-specific techniques, were adopted to investigate the interfacial spin state of antiferromagnetic Cr and spin polarization of Pt and Au. The XMCD measurements were carried out at beamlines BL25SU (soft X-rays) and BL39XU (hard X-rays) of the SPring-8 synchrotron radiation facility. The XMCD data were obtained from the difference between the XAS for left- and right-circularly polarized X-rays. Absorption signals were recorded using the total electron yield method at a bias voltage of −18 V for Cr and by the florescence method for Pt and Au. The incident angle of the X-rays was 10° from the surface normal for Cr and perpendicular to the film for Pt and Au. During all XMCD measurements, a magnetic field was applied in a direction perpendicular to the film plane.

RESULTS AND DISCUSSIONS

To study the influence of spacer layer materials on the magnetic properties in the perpendicular exchange-biased system, we used two types of films with different spacer layers of Pt and Au, which have the common bottom layer structure of Cr_2O_3/Pt/α-Al_2O_3.The structural quality of these bottom layers has to be identical for ensuring that observed effects on the magnetic properties result from the spacer layer itself. To this end, the AFM Cr_2O_3 layer was analysed by RHEED observations, XRD measurements, and XRR measurements. The RHEED images of the films with Pt and Au spacer layers and a Co layer thickness of 0.4 nm in Fig. 1 show that the Pt buffer and Cr_2O_3 layer produce very similar streaky patterns, though with superimposed elongated spots in the case of the Cr_2O_3 layer. These diffraction patterns suggest a fcc(111) structure for the Pt buffer layer and a corundum(0001) structure for the Cr_2O_3 layer.[22] Note that these diffraction patterns change with the electron azimuth, and that the un-equal spacing between streaks is the result of the textured structure of these layers. The different in-plane streak spacings for Cr_2O_3 seen in Figs. 1(a) and 1(b) are likely caused by charge-up of the insulating Cr_2O_3 layer due to the electron irradiation, and so are not considered to represent a significant difference in structural quality. Indeed, the X-ray diffraction peak positions of $Cr_2O_3(11\bar{2}0)$ and $Cr_2O_3(1\bar{1}04)$ were confirmed to be the same in both film types (data not shown).

In addition to the surface sensitive RHEED observations, the bulk sensitive high-angle XRD measurements

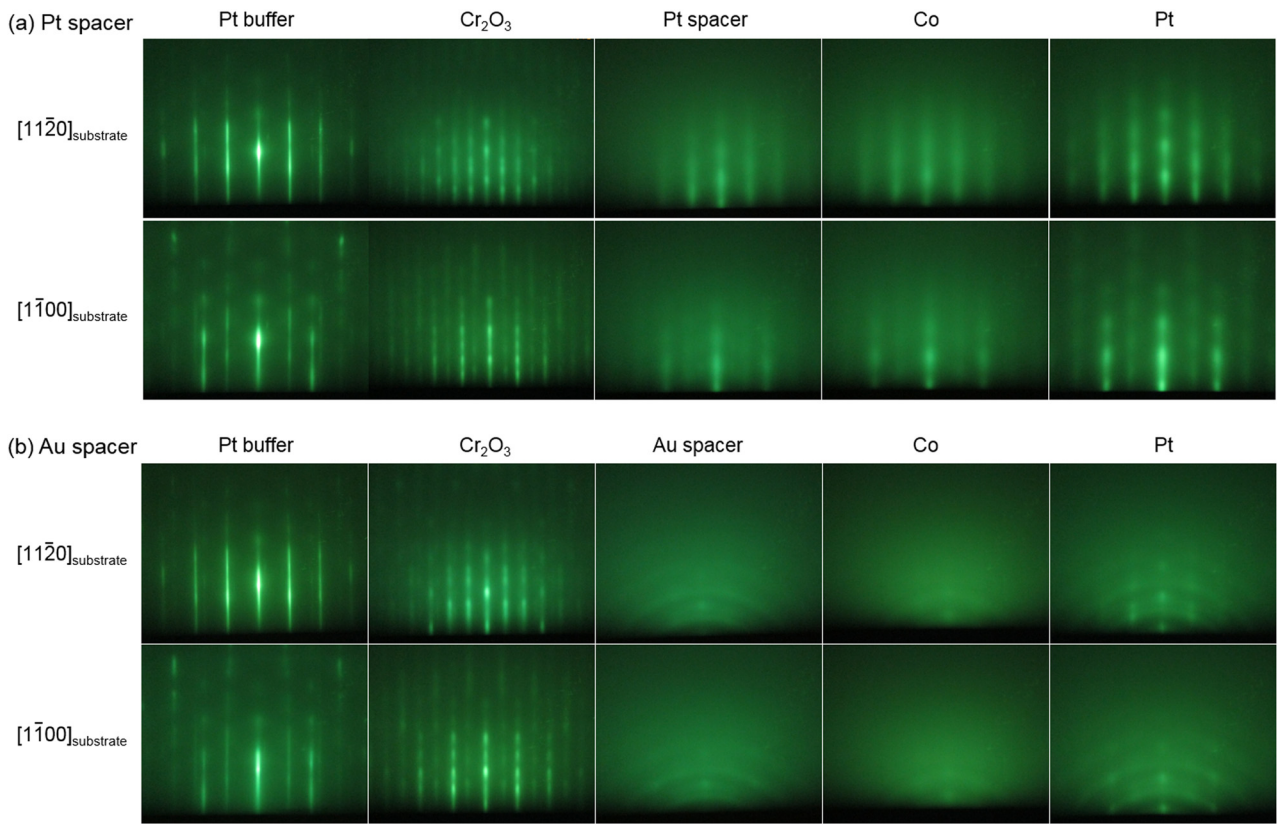

FIG. 1. RHEED images for films with a (a) Pt or (b) Au spacer layer. Electron azimuth was $[11\bar{2}0]$ and $[1\bar{1}00]$ of the α-Al_2O_3(0001) substrate for upper and bottom images, respectively. The images shown are for the films with a 0.4 nm-thick Co layer.

shown in Fig. 2 revealed that the structural quality of the Cr_2O_3 layer is very similar in both film types. It can be seen in this figure that in addition to the diffraction peaks originating from the substrate (indicated by *), peaks are observed at 2θ angles of 39.85° and 85.72° that correspond to Pt(111) or Cr_2O_3(0006), and Pt(222) or Cr_2O_3(00$\underline{12}$), respectively. Note that the diffractions from Pt(111) and Cr_2O_3(0006) are difficult to separate because they are so close (i.e., $2\theta = 39.76°$ for Pt(111) and 39.77° for Cr_2O_3(0006)), which is a problem that also occurs with the Pt(222) and Cr_2O_3(00$\underline{12}$) peaks. Nonetheless, many Laue fringes were observed around the diffraction peak of $2\theta = 39.85°$ (see the inset of Fig. 2). The coherent length estimated from the lattice spacing and number of lattice corresponds to the Pt buffer layer thickness. Furthermore, in the XRR profiles shown in Fig. 3, the clear oscillation was observed for both types of films suggesting the sharp interfaces. The roughness of the FM(Pt/Co/Pt or Pt/Co/Au)/Cr_2O_3 interface σ is also similar as summarized in Table I. According to the analysis, the roughness of the FM(Pt/Co/Pt or Pt/Co/Au)/Cr_2O_3 interface may be affected by the Co layer thickness rather than the spacer materials. (This may be because on the analysis, the inter-layer mixing in the Pt/Co/spacer layer or the discontinuous structure was not taken into account and the continuous layer was assumed, i.e., the precise film structure was difficult to model on the simulation. In any case, when we compare σ for the same Co thickness, σ is insensitive to the kind of different spacer material.) While the above results indicate that the fabricated Cr_2O_3 layers possess similar quality, the crystalline quality of the subsequent layer changes depending on the spacer layer material used. As shown in Fig. 1, the Pt spacer layer has a fcc(111)-oriented structure, whereas the Au spacer layer appears to be polycrystalline based on its ring pattern. This difference in crystalline quality means that the Co and Pt capping layers that are subsequently applied are fcc(111) in films with a Pt spacer, but polycrystalline in films with a Au spacer layer.

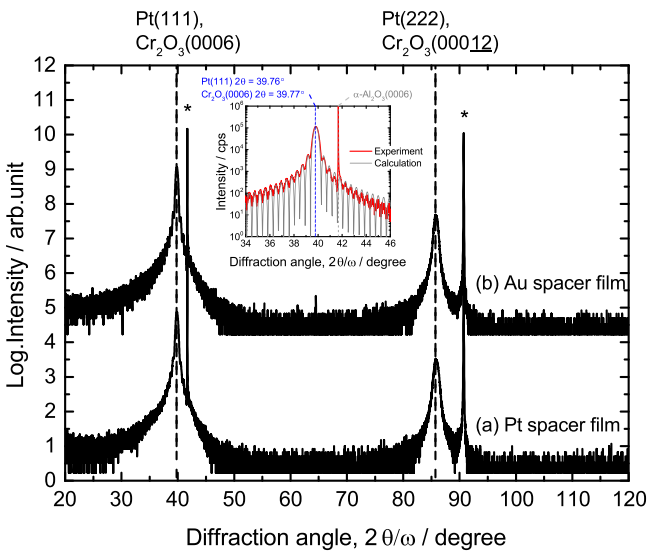

FIG. 2. XRD profiles of films with a (a) Pt or (b) Au spacer layer. Vertical dotted lines represent the diffraction position and diffraction peaks originating from the α-Al_2O_3(0001) substrate are marked by *. The inset shows an enlarged profile of the 24–46° 2θ range. Thick solid and thin dotted lines show experimental and calculated profiles using the Laue function. The profiles shown are for the films with a 0.4 nm-thick Co layer.

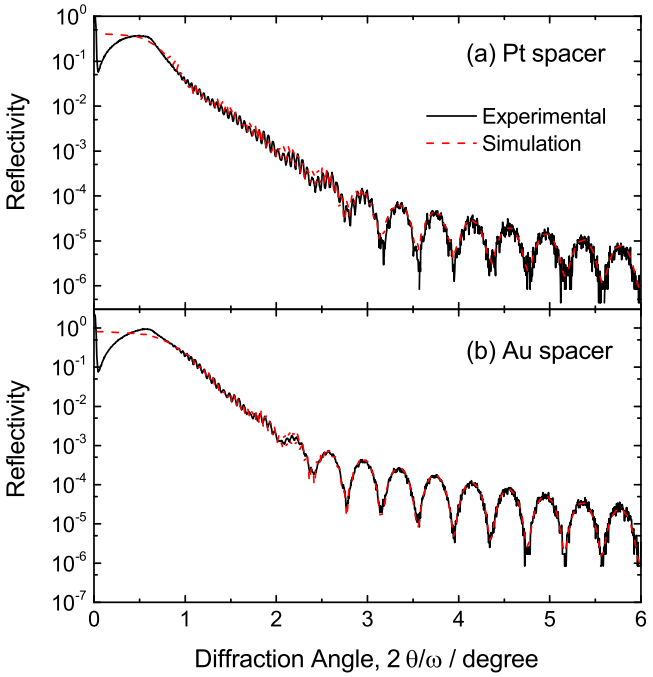

FIG. 3. XRR profiles of the films with a (a) Pt and (b) Au spacer layer. The black solid and red dotted lines represent the experimentally obtained and the simulated curves, respectively. The profiles shown are for the films with a 0.4-nm-thick Co layer.

Despite this, all of the films studied exhibited perpendicular magnetic anisotropy. From the magnetization curves shown in Fig. 4, it is also clear that all of the films had a high remanence ratio and low saturation field when a magnetic field was applied in a direction perpendicular to the film. However, as shown in Table I, the saturation magnetization M_S, uniaxial magnetic anisotropy energy density K_U, and in-plane saturation field H_S were different for the two film types. These parameters were estimated from the magnetization curves shown in Fig. 4 and the definition of K_U was shown in the note in Table I. M_S is almost the same for the films with the different Co thickness of 0.4 and 0.6 nm when the spacer materials are same; this indicates that reduction of Curie temperature for ultrathin regime of the Co layer[23] is negligible on M_S in our films around room temperature. The difference in M_S by the spacer materials is probably due to the induced magnetic moment of the spacer layer being higher with Pt than with Au.[24,25]

The difference in K_U and H_S by the spacer materials could be caused by the difference in crystalline quality between the two spacer layers described above. It is also possible that the difference in K_U and H_S might have been affected by the difference in typical magnetic anisotropy energy density at the Co(111)/Pt(111) interface (0.7–0.9 erg/cm^2) and Co/Au interface (0.4–0.5 erg/cm^2).[26] K_U and H_S also change with the Co layer thickness. This can essentially occur because the perpendicular magnetic anisotropy is caused by the interface magnetic anisotropy at the Co/Pt interface and/or the Co/Au interface; in an ideal case, K_U should increase with decreasing the Co thickness. However,

TABLE I. FM(Pt/Co/Pt or Pt/Co/Au)/Cr_2O_3 interface roughness (σ), saturation magnetization (M_S), perpendicular magnetic anisotropy energy density (K_U), in-plane saturation field (H_S), highest exchange magnetic anisotropy energy density (J_K), and estimated for the studied films. Note: (1) M_S and K_U were estimated on the assumption that magnetization is generated from the Co layer only. K_U was calculated using the formula, $K_U = (\int_0^{M_S} HdM)_{H//Film} - (\int_0^{M_S} HdM)_{H\perp Film}$. J_K was estimated using the relationship, $J_K = M_S{}^* t_{FM}{}^* H_{EX}$, where t_{FM} is a FM layer thickness and H_{EX} is an exchange bias field. For M_S, the room temperature value was used.

Film						
Co thickness (nm)	Spacer material	σ(nm)	M_S (emu/cc)	K_U (erg/cc)	H_S (kOe)	Highest J_K (erg/cm^2)
0.4	Pt	0.87	1550 ± 350	$(6.8 \pm 2.0) \times 10^6$	8.7 ± 1.8	0.11@180 K
0.4	Au	0.98	1240 ± 290	$(1.9 \pm 0.7) \times 10^6$	3.1 ± 0.9	0.21@160 K
0.6	Pt	0.49	1300 ± 280	$(7.5 \pm 2.2) \times 10^6$	11.6 ± 2.3	0.09@180 K
0.6	Au	0.39	1230 ± 130	$(4.5 \pm 0.9) \times 10^6$	7.3 ± 0.9	0.23@160 K

in our case, the Co layer thickness is below 4 monolayer in which Co may not be a continuous film and in this ultrathin regime, K_U can decrease for the low Co thickness as reported in earlier works.[27,28] Even in this case, the discontinuous structure of Co itself does not have an influence on the estimation of J_K. This is because the induced moment of both Pt and Au are coupled with the Co spins, and then the Pt/Co/Pt layer and the Pt/Co/Au layer behave like a single FM layer;

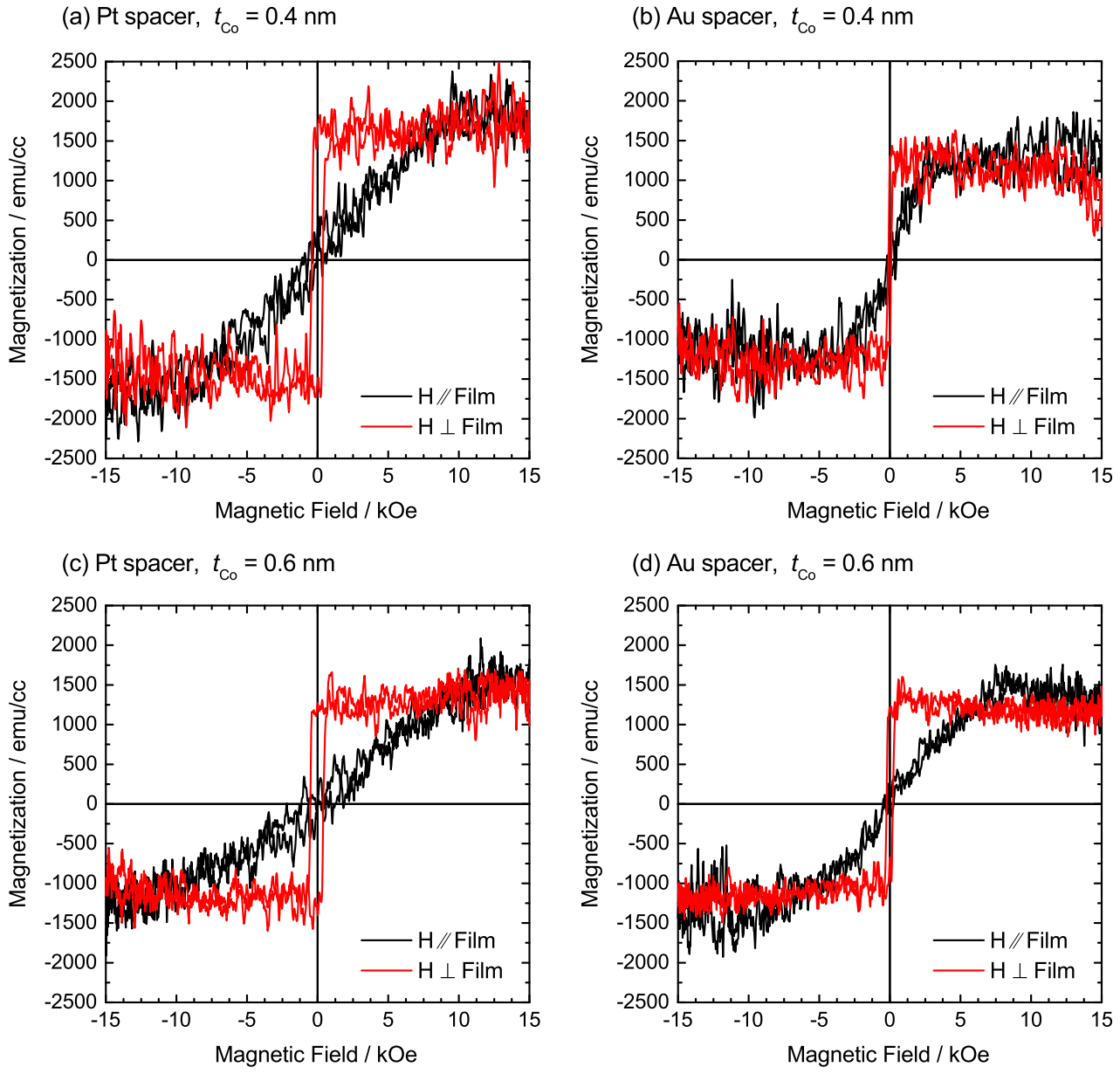

FIG. 4. Magnetization curves for films with a (a) and (c) Pt or (b) and (d) Au spacer layer and Co layer thickness of (a) and (b) 0.4 nm or (c) and (d) 0.6 nm. Red and black curves represent the magnetic field direction perpendicular and parallel to the film plane, respectively. All measurements were at room temperature.

the element-specific magnetization curves of Pt and Au is similar to that of the MOKE loop which is dominated by the Co spins.

Figure 5 shows the dependence of the perpendicular exchange bias field H_{EX} and coercivity H_C on temperature. The inset of Fig. 5(a) shows typical MOKE loop with definition of H_{EX} and H_C. With decreasing temperature, the exchange bias field of all of the studied films increases to a maximum at around 160–180 K, beyond which it decreases. This peak can be explained by interfacial spin canting at the $Cr_2O_3(0001)$ surface at temperatures below 160–180 K.[16] The peak temperature appears to be higher for the film with a Pt spacer, which considering the spin canting model, is likely to be due to a change in the interfacial Cr spin orientation. More significant is the difference in the absolute value of the exchange bias field between the two films. For example, with the 0.4-nm-thick Co films, those with a Au spacer layer (Fig. 5(b)) exhibited a high perpendicular exchange bias field of more than 4.2 kOe at its maximum (around 160 K), which yields J_K of 0.21 erg/cm^2 (also see Table I) and a coercivity lower than the exchange bias field at all temperatures studied below 285 K. At around 280 K, the coercivity was highly suppressed to less than 0.05 kOe, yet still maintained a perpendicular exchange bias field greater than 0.3 kOe. In contrast, the exchange bias field of the film with a Pt spacer layer (Fig. 5(a)) was just 1.8 kOe at its maximum (around 180 K), yielding J_K of 0.11 erg/cm^2 and a coercivity that exceeds the exchange bias field at temperatures above 270 K and below 120 K. A similar tendency was observed in the films with a 0.6-nm-thick Co film (Figs. 5(c) and 5(d)), but with a decrease in the absolute value of the perpendicular exchange bias field due to the increased Co layer thickness as confirmed by the fact that J_K is almost same for the different Co thickness (Table I). Thus, the coercivity is not as sensitive to the thickness of the Co layer as the perpendicular exchange bias field.

It is interesting to note that the film without a spacer layer had J_K that exceeded 0.4 erg/cm^2,[14] but the exchange bias did not persist up to the Néel temperature because of the low magnetic anisotropy of the Cr_2O_3 layer. Indeed, even with a 200 nm-thick Cr_2O_3 layer, the exchange bias disappears at around 120 K.[14] Details of the blocking temperature mechanism for this system can be found in previous papers.[9,10] The focus here is on the changes created in the perpendicular exchange bias field when using different spacer layer materials, particularly the degradation in perpendicular exchange bias that has been seen in films with a Pt spacer layer and how this relates to the interfacial spin orientation. Assuming that a Heisenberg-type exchange coupling occurs at the FM/AFM interface, the exchange coupling energy can be considered proportional to the scalar product of the interfacial FM and AFM spins. For the films studied in this paper, the magnetic moments induced in the spacer layers are regarded as the interfacial FM spins. According to previous reports, the spin polarization induced by the interfacial proximity effect with Co is about one order

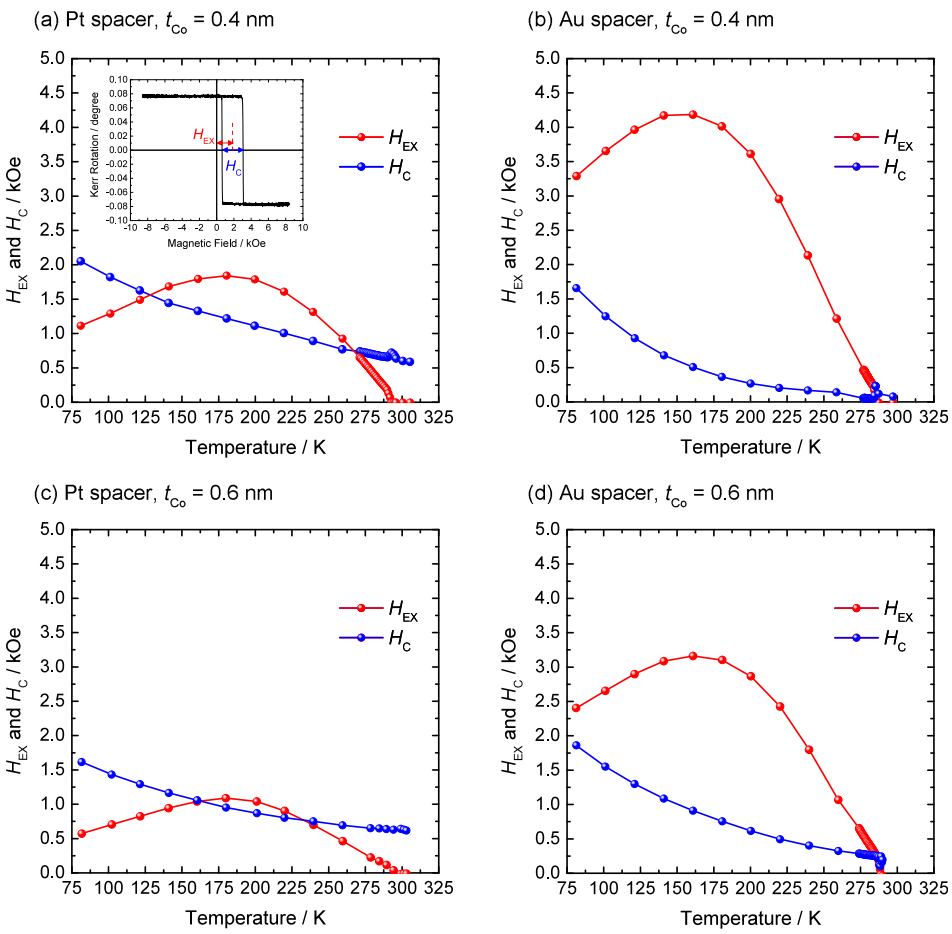

FIG. 5. Temperature dependence of perpendicular exchange bias field and coercivity for films with (a) and (c) Pt or (b) and (d) Au spacer layer and a Co layer thickness of (a) and (b) 0.4 nm or (c) and (d) 0.6 nm. Red and blue points represent the perpendicular exchange bias field and coercivity, respectively. The inset of (a) represents the typical MOKE loops exhibiting the exchange bias and in this figure, we show the definition of perpendicular exchange bias field and coercivity.

of magnitude higher for Pt ($\approx 0.6\,\mu_B$/atom)[24] than for Au ($\approx 0.031\,\mu_B$/atom).[25] Given this, the degradation in perpendicular exchange bias in films with a Pt spacer layer is likely caused by a reduction in the perpendicular component of the interfacial spins of either the FM or AFM spins; i.e., the spin canting from the surface normal.

The hard X-ray absorption spectra and hard XMCD spectra at the Pt $L_{2,3}$ edges of the films studied are shown in Fig. 6. Note that to induce a magnetic moment in the Pt, films with different stacking structures (e.g., Ru(3)/Pd(3)/Co(0.8)/Pt(0.5)/Cr_2O_3(70)/Pd(20)) were fabricated on α-Al_2O_3(0001) substrates to ensure that a Pt absorption signal was generated from the Pt spacer layer. As with previous reports, the Pt spacer layer was spin polarized and a sum rule analysis was used to obtain the effective spin moment $m_s^{eff} = m_{spin} - 7\,m_T = 0.54\,\mu_B$ and orbital moment $m_{orb} = 0.09\,\mu_B$ by assuming a hole number of 1.74.[24] The element specific magnetization curve of Pt shown in Fig. 6(b) also shows that the spin-polarized Pt exhibits clear perpendicular magnetic anisotropy with a remanence ratio at unity. We also confirmed that the XMCD intensity at the Pt L_3 edge exponentially decays according to $\exp(-t_{Pt}/\lambda)$ with the Pt thickness of t_{Pt} and the decay length of $\lambda = 0.42$ nm was similar to the result for Pt/Co bilayers with $\lambda = 0.41$ nm.[24] In addition, the XMCD intensity is almost constant in the temperature range of 180 to 300 K, across the Néel temperature of the Cr_2O_3 layer. These results suggest that the induction of the Pt moment is dominated by the exchange coupling with Co and the influence of the interfacial uncompensated Cr spin on the spin polarization of Pt is tiny. In fact, as shown in Fig. 6(b), the element-specific magnetization curve of Pt is very similar to the MOKE loop which is dominated by the Co contribution. Hence, even when the interfacial Cr spin is canted (see below), the induced Pt moment stays perpendicular to the film plane. Our XMCD measurements on the Au L_3 edge showed that the Au spacer is also spin-polarized but the observed XMCD intensity is ten-times smaller than that of Pt.[25] Nevertheless, we confirmed that similar to the Pt case, the element-specific magnetization curve of Au is similar to the MOKE loop indicating that the Au moment is mainly induced by the exchange coupling with Co; the induced Au moment is also perpendicular to the film plane.

To find the origin of the different perpendicular exchange bias fields in the AFM(Cr) spin orientations at the Pt/Cr_2O_3 and Au/Cr_2O_3 interfaces, the soft XMCD spectra at the Cr $L_{2,3}$ edges were obtained. These are shown in Fig. 7 along with the soft XMCD spectrum for a film without a spacer layer[29] for reference. The XMCD spectrum of the film with an Au spacer layer was similar to that of the film without a spacer layer, whereas the peak at the Cr L_3 edge indicated by the dotted line in Fig. 7 almost disappears at the Pt/Cr_2O_3 interface. In a previous report,[29] we suggested that

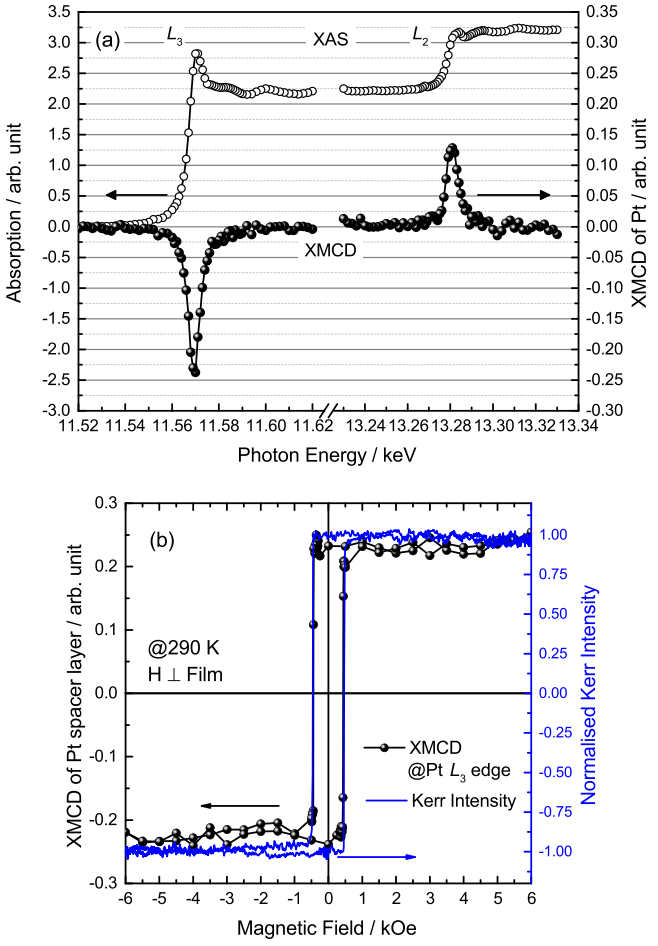

FIG. 6. (a) Hard X-ray absorption and magnetic circular dichroism spectra at Pt $L_{2,3}$ edges and (b) element specific magnetization curve measured at Pt L_3 edge with Pt spacer film. The XMCD intensity was normalized against the peak intensity of XAS. A Ru(3)/Pd(3)/Co(0.8)/Pt(0.5)/Cr_2O_3(70)/Pd(20) film was used to restrict the Pt signal from the Pt space layer. A magnetic field of 6 kOe was applied in a direction perpendicular to the film at a temperature of 290 K. In (b), the MOKE loop is also shown by the blue curve.

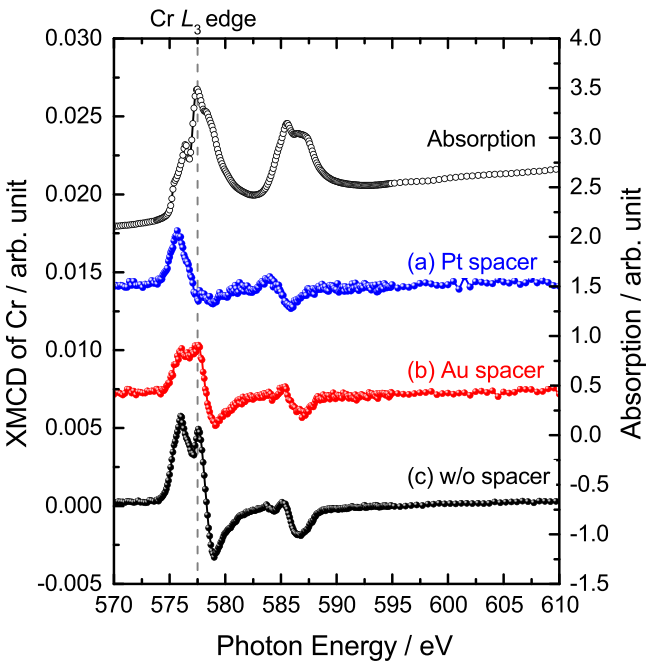

FIG. 7. Soft XMCD spectra at Cr $L_{2,3}$ edges for films with a (a) Pt or (b) Au spacer layer and 0.4 nm-thick Co film. The spectrum for a Pt(1.2)/Co(0.5)/Cr_2O_3(100)/Pt(20) film without a spacer is shown for reference in (c). XMCD intensity was normalized by the peak intensity at the Cr L_3 edge of XAS. A magnetic field of 19 kOe was applied perpendicular to the film and all measurements were made at room temperature. The XAS for the film without a spacer layer is shown on the right axis to identify the Cr L_3 edge.

the interfacial Cr spin orientation is sensitive to the peak intensity at the Cr L_3 edge; i.e., when the interfacial Cr spin is canted from the surface normal, the peak intensity at Cr L_3 should decrease. A similar change in the XMCD intensity at the Cr L_3 edge with respect to the Cr^{3+} spin orientation has also been reported in $MnCr_2O_4$ thin films.[30] Based on this change in the XMCD peak intensity, the spectra shown in Fig. 7 suggest that the interfacial Cr spin is canted at the Pt/Cr_2O_3 interface, but not at the Au/Cr_2O_3 interface. This difference can be explained by the magnetic anisotropy at the X(= Pt, Au, Co)/Cr_2O_3 interface.

It has been theoretically predicted that in-plane and perpendicular magnetic anisotropy is induced at Pt/Cr_2O_3 and Au/Cr_2O_3 interfaces, respectively.[31] In addition, we have reported that perpendicular magnetic anisotropy is induced at a Co/Cr_2O_3 interface;[32] in fact, the element-specific magnetization curve of the interfacial uncompensated Cr spins at the Co/Cr_2O_3 interface (data not shown) shows the square hysteresis for the perpendicular magnetic field. As shown above, both Co and induced Pt moments are perpendicular to the film plane because of the perpendicular magnetic anisotropy of the Pt/Co/Pt layer (see Fig. 4 and Table I). Compared with K_U of the Pt/Co/Pt layer, the magnetocrystalline anisotropy energy density of Cr_2O_3 is quite weak: at most $\approx 10^5$ erg/cc.[33] Then, the Cr_2O_3 layer undertakes the in-plane interfacial magnetic anisotropy by canting interfacial Cr spins from the surface normal. In contrast, the perpendicular magnetic anisotropy at Au/Cr_2O_3 and Co/Cr_2O_3 interfaces prevents the interfacial AFM spins canting from the surface normal, as evidenced by their similar XMCD spectra at Cr $L_{2,3}$. However, further investigation is still needed to quantitatively interpret the XMCD spectrum from uncompensated Cr spins, and this work is currently in progress.

SUMMARY

This investigation into the influence of Pt and Au spacer layers inserted at the Co/Cr_2O_3 interface on the perpendicular exchange bias field and the coercivity has shown that using Pt greatly degrades the perpendicular exchange bias field, whereas Au spacers can maintain a high perpendicular exchange bias and prevent an increase in coercivity. Based on their respective interfacial spin orientations, it is suggested that the degradation in perpendicular exchange bias caused by the Pt spacer layer is the result of interfacial spin canting of the AFM Cr spins that is induced by in-plane interface magnetic anisotropy at the Pt/Cr_2O_3 interface.

ACKNOWLEDGMENTS

The XAS and XMCD experiments were performed at the SPring-8 synchrotron radiation facility with the approval of JASRI (Proposal Nos. 2013A1751, 2013B1267, 2015A0079, 2015B0079, 2016A0079, and 2016B0079). This work was partly supported by JSPS KAKENHI (Grant Nos. 16H03832 and 16H02389), the ImPACT program of the Council for Science, Technology and Innovation (Cabinet Office, Government of Japan), the Izumi Scientific Foundation and the Photonics Advanced Research Center (PARC) at Osaka University.

[1]B. Dieny, V. S. Speriosu, S. Metin, S. S. P. Parkin, B. A. Gurney, P. Baumgart, and D. R. Wilhoit, J. Appl. Phys. **69**, 4774 (1991).
[2]W. H. Meikjejohn and C. P. Bean, Phys. Rev. **102**, 1413 (1956).
[3]J. Nogués and I. K. Schuller, J. Magn. Magn. Mater. **192**, 203 (1999).
[4]A. E. Berkowitz and K. Takano, J. Magn. Magn, Mater. **200**, 552 (1999).
[5]C. Leighton, J. Nogués, B. J. Jönsson-Åkerman, and I. K. Schuller, Phys. Rev. Lett. **84**, 3466 (2000).
[6]S. Maat, K. Takano, S. S. P. Parkin, and E. E. Fullerton, Phys. Rev. Lett. **87**, 087202 (2001).
[7]M. H. Dung, N. P. Thuy, N. A. Tuan, N. T. Long, and N. N. Phunc, J. Magn. Magn. Mater. **320**, 3334 (2008).
[8]H. Takahashi, M. Tsunoda, and M. Takahashi, IEEE Trans. Magn. **48**, 4347 (2012).
[9]Y. Shiratsuchi, T. Fujita, H. Oikawa, H. Noutomi, and R. Nakatani, Appl. Phys. Express **3**, 113001 (2010).
[10]Y. Shiratsuchi and R. Nakatani, Mater. Trans. **57**, 781 (2016).
[11]F. Carcia, J. Sort, B. Rodmaq, S. Auffret, and B. Dieny, Appl. Phys. Lett. **83**, 3537 (2016).
[12]J. Sort, F. Carcia, B. Rodmaq, S. Auffret, and B. Dieny, J. Magn. Magn. Mater. **272–276**, 355 (2004).
[13]Y. Shiratsuchi, T. Fujita, H. Noutomi, H. Oikawa, and R. Nakatani, IEEE Trans. Magn. **47**, 3909 (2011).
[14]Y. Shiratsuchi, Y. Takechi, K. Toyoki, Y. Nakano, S. Onoue, C. Mitsumata, and R. Nakatani, Appl. Phys. Express **6**, 123004 (2013).
[15]P. Borisov, A. Hochstrat, X. Chen, W. Kleemann, and C. Binek, Phys. Rev. Lett. **94**, 117203 (2005).
[16]X. He, Y. Wang, N. Wu, A. N. Caruso, E. VVescovo, K. D. Belashchenko, P. A. Dowben, and C. Binek, Nat. Mater. **9**, 579 (2010) and supplemental information.
[17]T. Ashida, M. Oida, N. Shimomura, T. Nozaki, T. Shibata, and M. Sahashi, Appl. Phys. Lett. **104**, 152409 (2014).
[18]K. Toyoki, Y. Shiratsuchi, T. Nakamura, C. Mitsumata, S. Harimoto, Y. Takechi, T. Nishimura, H. Nomura, and R. Nakatani, Appl. Phys. Express **7**, 114201 (2014).
[19]T. Ashida, M. Oida, N. Shimomura, T. Nozaki, T. Shibata, and M. Sahashi, Appl. Phys. Lett. **106**, 132407 (2015).
[20]K. Toyoki, Y. Shiratsuchi, A. Kobane, C. Mitsumata, Y. Kotani, T. Nakamura, and R. Nakatani, Appl. Phys. Lett. **106**, 162404 (2015).
[21]X. Chen, A. Hochstrat, P. Borisov, and W. Kleemann, Appl. Phys. Lett. **89**, 202508 (2006).
[22]A. Stierle, Th. Koll, and H. Zabel, Phys. Rev. B **58**, 5062 (1998).
[23]D. Chiba, S. Fukami, K. Shimamura, N. Ishiwata, K. Kobayashi, and T. Ono, Nat. Mater. **10**, 853 (2011).
[24]M. Suzuki, H. Muraoka, Y. Inaba, H. Miyagawa, N. Kawamura, T. Shimatsu, H. Maruyama, N. Ishimatsu, Y. Isohama, and Y. Sonobe, Phys. Rev. B **72**, 054430 (2005).
[25]F. Wilhelm, M. Angelekeris, N. Jaouen, P. Poulopoulos, E. Th Papaioannou, Ch. Muller, P. Fumagalli, A. Rogalev, and N. K. Flevaris, Phys. Rev. B **69**, 220404(R) (2004).
[26]M. T. Johnson, P. J. H. Bloemen, F. J. A. den Broeder, and J. J. de Vries, Rep. Prog. Phys. **59**, 1409 (1996) and references therein.
[27]F. J. A. den Broeder, W. Hoving, and P. J. H. Bloemen, J. Magn. Magn. Mater. **93**, 562 (1991).
[28]W. B. Zeper, F. J. A. Greidanus, P. F. Carcia, and C. R. Fincher, J. Appl. Phys. **65**, 4971 (1989).
[29]Y. Shiratsuchi, H. Noutomi, H. Oikawa, T. Nakamura, M. Suzuki, T. Fujita, K. Arakawa, Y. Takechi, H. Mori, T. Kinoshita, M. Yamamoto, and R. Nakatani, Phys. Rev. Lett. **109**, 077202 (2012).
[30]G. van Laan, R. V. Chopdekar, Y. Suzuki, and E. Arenholz, Phys. Rev. Lett. **105**, 067405 (2010).
[31]M. Ikuta and K. Nakamura, in *59th Annual Conference on Magnetism and Magnetic Materials* (2014), p. CQ-11.
[32]Y. Shiratsuchi, H. Oikawa, S. Kawahara, Y. Takechi, T. Fujita, and R. Nakatani, Appl. Phys. Express **5**, 043004 (2012).
[33]S. Foner, Phys. Rev. **130**, 183 (1963).